Radio Science, Volume 34, Number 6, Pages 1349–1359, November–December 1999

Investigation of mode interaction on planar dielectric waveguides with loss and gain

George W. Hanson

Department of Electrical Engineering and Computer Science, University of Wisconsin-Milwaukee

Alexander B. Yakovlev

Department of Electrical and Computer Engineering, North Carolina State University, Raleigh

Abstract. On lossless isotropic planar waveguides the discrete proper modes of propagation form independent transverse electric and transverse magnetic sets such that there is no mode coupling or interaction between modes. In the event of material loss or gain, mode interactions are possible, leading to a complicated spectrum and apparent nonuniqueness of the modes. In this paper we analyze for the first time the cause of these modal interactions by studying the simplest canonical planar waveguide which exhibits these effects, the symmetric-slab waveguide. We show that mode interactions are due to the migration of complex-frequency-plane branch points associated with specific wave phenomena, with varying loss or gain. As these singularities move near the real-frequency axis they influence the modal behavior for time-harmonic (real-valued) frequencies, crossing the real axis at some critical value of loss or gain. It is shown that as time-harmonic frequency varies, passing above, below, or through these branch points results in different modal behavior. Passing above or below, and near to, the branch point yields mode coupling behavior, while passing through the branch point results in modal degeneracy. The result of this branch point migration is that the association of a particular mode with a certain branch of the dispersion function depends not only on the value of material loss or gain, but also on the order in which physical parameters of the problem are varied. Three different branch point types are identified and discussed, which leads to an understanding of the relevant wave phenomena and to a method for organizing the mode spectrum in a consistent and unique manner. While many of the observations described here are based on careful numerical analysis of the transverse magnetic modes existing on a certain symmetric-slab waveguide, the described phenomena are reasonably expected to be generally found in other open dielectric waveguiding structures.

1. Introduction

Planar dielectric waveguides play a fundamental role as a building block for integrated optical devices and as substrates for microwave and millimeter-wave integrated circuits. The fact that a lossless planar waveguide has a discrete and continuous spectrum with certain orthogonality properties is well known [*Marcuse*, 1991; *Collin*, 1991]. Source-driven and discontinuity problems can be analyzed by expanding the unknown field quantities in the complete set of discrete and continuous modal eigenfunctions associated with the waveguide. The discrete modes are particularly important in waveguiding problems. The proper discrete modes physically represent propagating surface waves bound to the waveguiding structure. The improper discrete modes, or leaky modes, are useful in representing the radiation field (continuous spectrum) in certain spatial regions. Therefore identification and classification of the discrete surface-wave modes are important in understanding the operation of optical waveguides and planar electronic structures.

In practical applications of optical devices, as well as in waveguiding applications in other frequency regimes, planar waveguides may be utilized with strongly lossy layers, or layers exhibiting gain, for example, in laser

Paper number 1999RS900096.
0048-6604/99/1999RS900096$11.00

applications. For very small loss or gain, the discrete modes are slightly perturbed from those of the lossless case, and techniques developed for lossless planar waveguides may be applied. In the event of moderate or large loss or gain, the discrete modes become significantly perturbed such that classification of the modes becomes difficult. This classification difficulty arises not only because modes become coupled together, but also because the order in which physical parameters of the problem are varied affects the modal trajectories in wavenumber space during computer simulation [*Van Stralen* et al., 1997]. Modal characteristics and the apparent nonuniqueness of modes on some lossy planar waveguides have been investigated by *Van Stralen* et al. [1997, and references therein], although the causes of the modal interactions were not identified.

In this paper we analyze a symmetric-slab waveguide with loss and gain to show that modal interactions and the apparent nonuniqueness of the mode spectrum are due to the migration of complex-frequency-plane branch points with varying loss or gain. This behavior is explained by first considering the locations of various singularities and special points in the complex frequency plane for the lossless case, including a description of modal (dispersion) behavior as frequency is varied along the real axis. Next, the role of complex-frequency-plane singularities is explained by considering various paths of frequency variation in the complex plane. It is shown that the singularities responsible for mode coupling for the lossy (or gain) case reside off the real axis in the complex-frequency plane for lossless waveguides but migrate across the real-frequency axis as loss or gain is varied. As these singularities move near the real axis they are shown to influence the modal behavior for the time-harmonic (real-valued) frequencies of interest. The effect of passing above, below, or through these branch points as frequency is varied is analyzed. A method for determining the location of these singularities is presented, and loss/gain regimes are identified with various mode interaction problems. It is shown that the mode spectrum is indeed uniquely defined if the path of variation in the parameter space of the problem is well defined.

Note that in another recent paper [*Yakovlev and Hanson*, 1999] complex-frequency-plane branch points have been identified and associated with mode coupling. In that paper the result of an investigation on the effect of loss was also presented, leading to the identification of two separate mode interaction regimes. The branch points discussed in that paper are associated with structures which, in the lossless case and for real-valued frequencies, inherently admit coupled modes and are completely different from the branch points considered here.

2. Discussion and Results

Consider the symmetric-slab waveguide shown in Figure 1. The structure is infinite in the x and z directions, the latter being the direction of wave propagation. We consider two-dimensional wave propagation, with no variation occurring in the transverse (x) direction. Propagation governed by the factor $e^{j(\omega t - \lambda z)}$ is assumed; note that λ represents the modal propagation constant rather than wavelength.

Procedures to develop the governing transcendental eigenvalue equations for discrete modes which may be supported by the structure are well known [*Marcuse*, 1991; *Collin*, 1991] and will not be discussed here. To summarize, four types of discrete modes may exist. With respect to the axis of propagation, transverse electric (TE^z) and transverse magnetic (TM^z) modes may occur. Each type of mode can be divided into even and odd modes, designations referring to symmetry of the transverse component of field (E_x for TE^z modes and H_x for TM^z modes). Thus four independent transcendental eigenvalue equations may be derived for the generally lossy case, indicating that TE^z and TM^z modes will not interact, nor will even and odd modes interact within a mode class. The only interaction between modes may occur for modes having the same symmetry (even or odd) and polarization (TE^z or TM^z), although mode degeneracies may otherwise occur. These degeneracies may be broken by perturbing the symmetry of the waveguide, for example, by introducing material anisotropy or chirality, or structural perturbations such as the addition of material ridges. It is shown by *Yakovlev and Hanson* [1998] that these modal degeneracies are unstable with respect to perturbations of this type, the presence of which leads to modal coupling. Such effects will not be considered here.

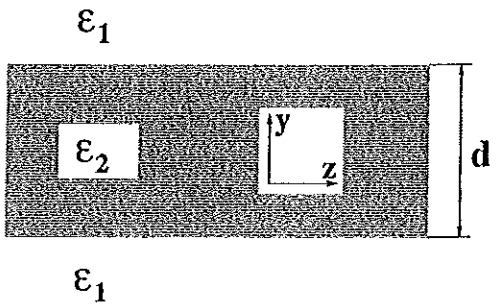

Figure 1. Symmetric-slab waveguide geometry.

In this work we will concentrate on even TM^z modes of the symmetric-slab waveguide, although it is likely that some of these results will carry over to the other three classes of modes. The even TM^z modes are precisely those TM^z modes which may propagate on a grounded dielectric slab, and so these modes are important in common planar electronic technology.

For the structure depicted in Figure 1, TM^z-even modes are governed by the dispersion equations

$$H(\lambda,\omega)=\frac{\epsilon_2}{\epsilon_1}p_1+p_2\tanh\left(p_2\frac{d}{2}\right)=0, \tag{1}$$

where $p_j=\sqrt{\lambda^2-(n_j\omega/c)^2}$, $n_j=\sqrt{\epsilon_j/\epsilon_0}$, $j=1,2$, $c=1/\sqrt{\mu_0\epsilon_0}$, ω is the radian frequency, and λ is the modal propagation constant. Equation (1) is even in p_2 and ω, but the sign of the square root for p_1 must be chosen carefully, as branch points occur in the λ plane at $\lambda=\pm n_1\omega/c$. In this work the usual hyperbolic branch cuts which separate the proper (plus sign) and improper (minus sign) Riemann sheets [*Collin*, 1991] in the λ plane will be chosen. These cuts are defined by $\mathrm{Re}\{p_1\}=0$, leading to

$$Im\{\lambda\}=\frac{Im\{n_1\omega\}\,Re\{n_1\omega\}}{c^2Re\{\lambda\}}$$
$$|Re\{\lambda\}|<\frac{1}{c}|Re\{n_1\omega\}|. \tag{2}$$

The dispersion equation (1) implicitly determines the dispersion function $\lambda_m(\Omega)$, $m=0,1,2,\ldots$ where $\Omega=\{\omega,d,\epsilon_1,\epsilon_2\}$ represents the four-dimensional parameter space of the dispersion function. When the space of parameters is real, i.e., $\Omega\in\mathbb{R}^4$, the dispersion function is well understood. Independent discrete modes exist, which may be found numerically from (1). A well-known graphical procedure [*Collin*, 1991] can be used to verify that the proper modes can be identified with a finite set $m=0,2,4,\ldots,M$ on the proper Riemann sheet for any finite frequency, such that the symbolic representation $\lambda_m(\Omega)$ is appropriate. Improper modes form a countably infinite set on the improper Riemann sheet [*Collin*, 1991] and can also be determined from (1) with the appropriate definition of the square root in p_1. If the parameter space is regarded as generally complex, $\Omega\in\mathbb{C}^4$, the dispersion function is exceedingly complicated. In fact, it is shown below and briefly discussed by *Niu and Felsen* [1993] that in this case, every "mode" is analytically continuous to every other "mode." It is this property of the dispersion function which leads to the modal interaction of interest here. In the following, the subscript notation $\lambda_m(\Omega)$ will be retained as the parameter space is continued into the complex domain in order to aid identifying modes with their counterparts for real parameter space. In this case, however, for a mode $\lambda_m(\Omega)$ the subscript value is actually not only a function of the parameter space, $\lambda_{m(\Omega)}(\Omega)$, but also depends on the order in which parameters are varied.

In order to understand the source of mode interactions induced by material loss or gain, it is convenient to first consider the locations of branch points and cutoff frequencies in the complex-frequency-plane for the lossless case. Figure 2 illustrates those features relevant to understanding the behavior of the TM^z-even modes for the right-half frequency plane. This figure is quite complicated, and considerable discussion will follow, providing a through explanation of all depicted features. We will start with a discussion of the frequency-plane features located on the real-frequency axis.

First consider the locations of the modes at $\omega=0$. The dominant (TM_0) mode, $\lambda_0^{(+)}$, is at the origin of the λ plane on the proper sheet. All of the other modes, TM_m, $m=2,4,6,\ldots$, begin as conjugate pairs on the improper Riemann sheet at

$$\lambda_m^{(-)}=\mp j(m-1)\frac{\pi}{d}+\frac{1}{d}\ln\left[\frac{\left(\frac{n_2}{n_1}\right)^2+1}{\left(\frac{n_2}{n_1}\right)^2-1}\right] \tag{3}$$

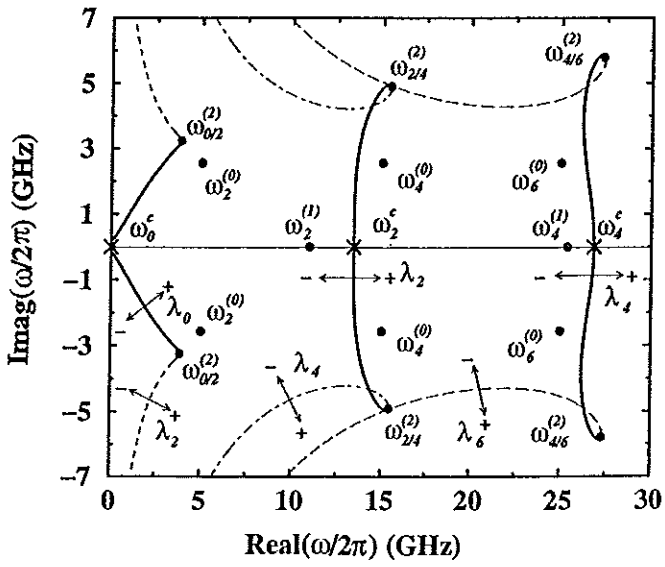

Figure 2. Complex-frequency-plane singularities (dots) and generalized cutoff-frequency loci (solid and dashed lines) for the TM^z-even modes of the symmetric-slab waveguide depicted in Figure 1, with $\epsilon_1=\epsilon_0$, $\epsilon_2=2.25\,\epsilon_0$, and $d=2$ cm. Cutoff frequencies are denoted by crosses.

m=2,4,6..., which is obtained from (1) under the restriction ω=0. The designation $\lambda_m^{(+)/(-)}$ indicates the mth mode on the proper (plus sign) or improper (minus sign) sheet. Since the structure is composed of reciprocal media and is longitudinally invariant, $-\lambda_m$ are also modes of the structure. For lossless media and ω real-valued or imaginary, $\overline{\lambda}_m$ are also modes of the structure, where the overbar denotes complex conjugate. The locations of the modes in the λ plane for ω=0 are shown in Figure 3. Each mode represents a unit multiplicity root of (1), except $\lambda_0^{(+)}$, which has multiplicity two (a double root). For convenience in the following, reference will be made to mode pairs $(\lambda_m^{(-)}, \overline{\lambda}_m^{(-)})$, which represent the conjugate pairs $(\lambda_m^{(-)}, \overline{\lambda}_m^{(-)})$ and $(-\lambda_m^{(-)}, -\overline{\lambda}_m^{(-)})$ that exist at ω=0 and for real frequencies such that $\omega<\omega_m^{(1)}$ as explained below, and their continuations to arbitrary complex frequency. Therefore $\overline{\lambda}_m^{(-)}$ is the mode which for a lossless structure and sufficiently low real-valued frequencies is the conjugate of $\lambda_m^{(-)}$.

Modal variation with real frequency is depicted in Figure 4. As frequency is increased from ω=0 along the positive real ω axis, $\lambda_0^{(+)}$ moves away from the origin along the real λ axis, staying on the proper sheet (for ω=0 in Figure 4, $\lambda_0^{(+)}$ does not appear at the origin due to the normalization with respect to frequency). The modes $\pm(\lambda_m^{(-)}, \overline{\lambda}_m^{(-)})$ for m>0 follow a trajectory maintaining conjugate symmetry (imaginary part not shown in Figure 4) until the point $\omega_m^{(1)}$ is reached. At this point the modes meet on the real λ axis, temporarily forming a second-order root of (1). Between $\omega_m^{(1)}$ and ω_m^c the modes move in different directions along the real λ axis. The mode which moves away from the origin remains on the improper Riemann sheet for all real frequency such that $\omega>\omega_m^{(1)}$. The other mode, which initially moves toward the origin along the real λ axis, passes through the λ-plane branch point $\lambda=\pm n_1\omega/c$ at $\omega=\omega_m^c$, i.e., $\lambda_m(\omega_m^c)=\pm n_1\omega_m^c/c$, onto the proper λ-plane Riemann sheet. As frequency further increases, that mode (the usual surface-wave mode) continues to move along the real λ axis, becoming asymptotic to $\pm n_2\omega/c$ for large frequency.

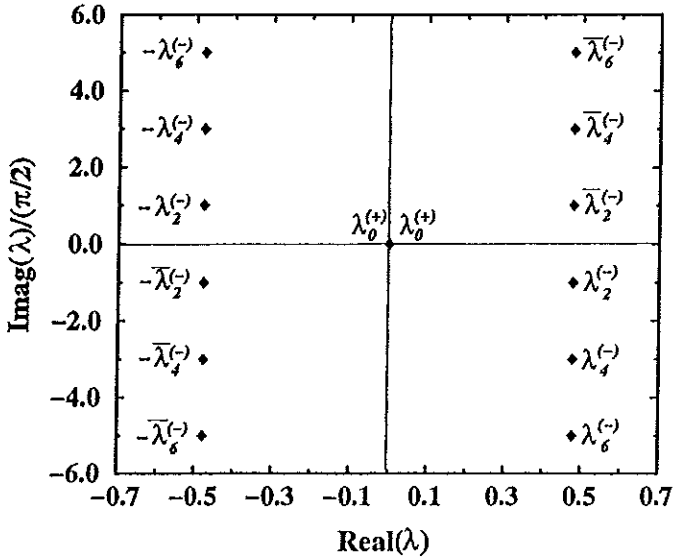

Figure 3. Location of the modal propagation constants in the complex λ plane for ω=0 and $\epsilon_1=\epsilon_0, \epsilon_2=2.25\,\epsilon_0$, and d=2 cm. All modes are on the improper (minus sign) sheet except $\lambda_0^{(+)}$.

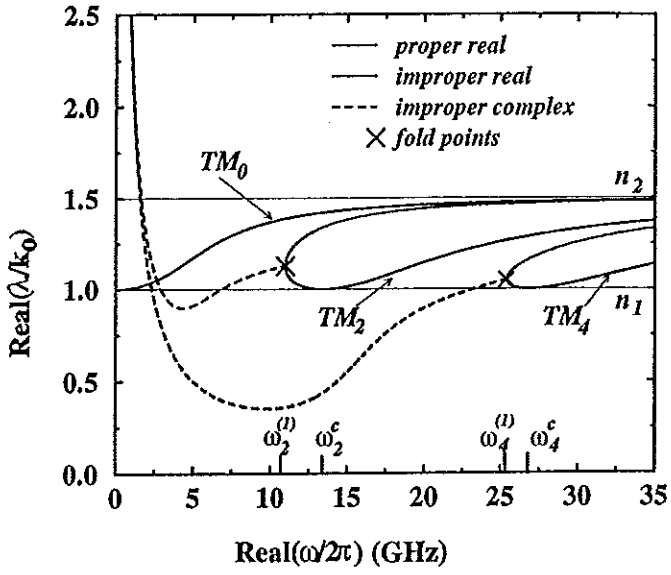

Figure 4. Dispersion behavior for the first three TM^z-even modes of Figure 1 for $\epsilon_1=\epsilon_0, \epsilon_2=2.25\,\epsilon_0$, and d=2 cm. The complex modes occur in conjugate pairs; the imaginary propagation constant is not shown.

In summary, for m>0 and real-valued frequency variation with $\omega<\omega_m^{(1)}$, both modes in the pair $\pm(\lambda_m^{(-)}, \overline{\lambda}_m^{(-)})$ are complex-valued, with $\pm\overline{\lambda}_m^{(-)}=\pm\lambda_m^{(-)}$. For the frequency range $\omega_m^{(1)}<\omega<\omega_m^c$ both modes in the pair $\pm(\lambda_m^{(-)}, \overline{\lambda}_m^{(-)})$ are real-valued on the improper-sheet, and for $\omega>\omega_m^c$ both modes in the pair are real-valued, one existing on the proper sheet and one on the improper sheet, denoted as $\pm(\lambda_m^{(+)}, \lambda_m^{(-)})$.

The points $\omega_m^{(1)}$ and ω_m^c are obviously special points for the mth mode. Indeed, ω_m^c is the cutoff frequency, above which one mode of the pair $(\lambda_m^{(-)}, \overline{\lambda}_m^{(-)})$ goes above cutoff (changes from the improper to the proper Riemann

sheet). The cutoff frequency [*Collin*, 1991] can easily be determined from the condition $p_1=0$ together with (1), leading to

$$\omega_m^c = \left(\frac{m\pi c}{d\sqrt{n_2^2 - n_1^2}}, 0 \right) \tag{4}$$

m=0,2,4,... for the even TM^z modes, at which point a mode $\lambda_m(\omega)$ of (1) passes through the λ-plane branch point at $\lambda = \pm n_1\omega/c$. It can be shown that the cutoff frequency ω_m^c is not a branch point of $\lambda_m(\Omega)$.

The point $\omega_m^{(1)}$, which could be called the leaky-wave cutoff frequency since below this frequency one mode of the pair is the traditional below-cutoff leaky mode, denotes where the modes $(\lambda_m^{(-)}, \lambda_m^{(-)})$ coalesce to form a second-order root of (1). The point $\omega_m^{(1)}$ is a first-order branch point for the pair [*Hanson and Yakovlev*, 1998], such that one complete rotation about $\omega_m^{(1)}$ results in an interchange of modes in the pair. In this way, as frequency is increased along the real axis, higher-order modes meet momentarily along the real λ axis and then separate. One will remain on the improper sheet, whereas the other mode will pass onto the proper sheet through the branch point at $\lambda = \pm n_1\omega/c$, becoming an ordinary, proper, surface-wave mode.

When one allows frequency to be complex, in this case to aid in the understanding of mode coupling, many interesting features emerge. First, we introduce here the concept of a generalized cutoff frequency. The usual definition of modal cutoff in open boundary waveguides is obtained by considering the real-valued frequency at which a proper mode moves through a λ-plane branch point to become an improper mode (residing on the improper sheet). Of course, it is not necessary for a mode to pass through the λ-plane branch point to move between Riemann sheets. Any frequency path that causes the mode to cross the proper hyperbolic λ-plane branch cuts (equation (2)) will result in a transition between proper and improper λ-plane Riemann sheets. The frequency at which the mode crosses the cut could be called a generalized cutoff frequency. In the case of the mode passing through the branch point itself, this reduces to the usual definition of cutoff frequency. These generalized cutoff frequencies will satisfy (1), along with the additional condition $\mathrm{Re}\{p_1\}=0$. Unfortunately, this does not lead to an explicit formula for the locus of generalized cutoff frequencies, but rather yields three real equations in three real unknowns (ω_r, ω_i, and λ_r or λ_i). The loci of points for several low-order TM^z modes were determined numerically for the slab under consideration and are shown in Figure 2. The solid lines (passing through the ordinary cutoff points ω_m^c) represent the locus of frequencies at which one of the modes from the mth mode pair $(\lambda_m^{(-)}, \lambda_m^{(-)})$ crosses the λ-plane branch cuts (indicated by the double-headed arrow in the figure). The other mode remains on the improper sheet. Which mode of the pair passes onto the proper sheet depends upon the path in the frequency plane. Starting at ω=0 and passing under $\omega_m^{(1)}$ results in the first- and third- quadrant modes passing onto the proper Riemann sheet, whereas passing above $\omega_m^{(1)}$ results in the fourth- and second-quadrant modes passing onto the proper Riemann sheet. Note that this notion of a generalized cutoff loci is not unique in that other λ-plane branch cuts will result in other generalized cutoff frequency loci, all passing through ω_m^c for the mth mode. The choice shown here, consistent with the usual hyperbolic λ-plane branch cuts, is perhaps the most physically meaningful.

Near the terminus of the solid lines in Figure 2 lie branch points that separate the mth mode from the negative of the $(m+2)$th mode (separates $\lambda_m(\Omega)$ and $-\lambda_{m+2}(\Omega)$), designated as $\omega_{m/m+2}^{(2)}$. These points connect the mth and $(m+2)$th modes such that a complete rotation about $\omega_{m/m+2}^{(2)}$ results in the smooth interchange of the $\pm m$th and $\mp(m+2)$th modes. As such, $\omega_{m/m+2}^{(2)}$ are first-order branch points for the mth and $-(m+2)$th modes.

The dashed lines represent the locus of points where other modes change Riemann sheets, as indicated in the figure. For instance, starting at ω=0 and crossing the appropriate dashed contour causes $\lambda_4^{(-)}$ to cross from the improper to the proper Riemann sheet in the λ plane. Because of the $\omega_{2/4}^{(2)}$ branch point, however, that mode cannot smoothly become the usual above-cutoff $\lambda_4^{(+)}$ mode for real frequencies. Indeed, as seen in Figure 5a, starting with $\lambda_4^{(-)}$ at point A and following the indicated path to point B smoothly changes the mode into the $\lambda_2^{(+)}$ mode above cutoff $(\lambda_4^{(-)} \rightarrow \lambda_4^{(+)} \rightarrow -\lambda_2^{(+)})$. In a similar manner, Figure 5b shows that starting with the mode $\lambda_2^{(-)}$ at point A and following the indicated path to point B results in a smooth conversion of the $\lambda_2^{(-)}$ mode into the $\lambda_6^{(-)}$ mode $(\lambda_2^{(-)} \rightarrow -\lambda_4^{(-)} \rightarrow \lambda_6^{(-)})$, where the mode has remained on the improper Riemann sheet (still below cutoff). Note that some labels in the upper half plane of Figure 2 are omitted for clarity; corresponding labels in the lower half plane apply.

Other frequency-plane branch points occur at frequencies where the modes λ_m and $-\lambda_m$ meet at λ=0 [*Hanson and Yakovlev*, 1998; *Haddon*, 1986]. These frequencies can be determined explicitly from enforcing the condition λ=0 in (1), resulting in

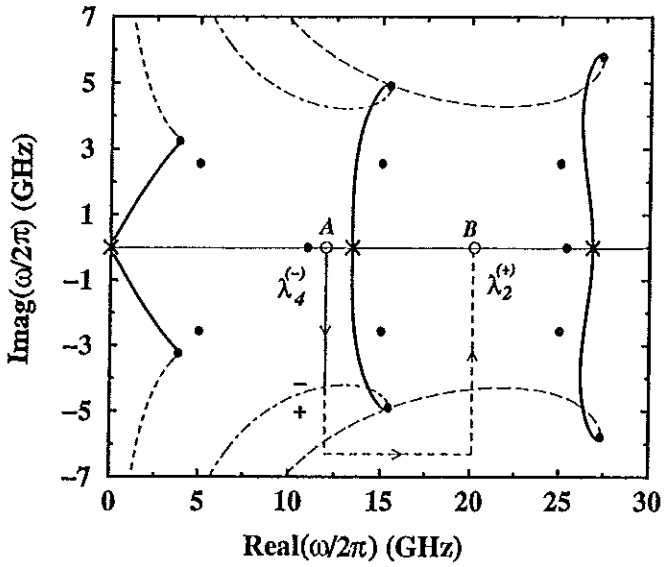

Figure 5a. Example of a complex-frequency-plane path which results in the transformation of the $\lambda_4^{(-)}$ mode into the $\lambda_2^{(+)}$ mode.

$$\omega_m^{(0)} = (m-1)\frac{c\pi}{n_2 d} \pm j\frac{c}{n_2 d}\ln\left[\frac{1+\frac{n_1}{n_2}}{1-\frac{n_1}{n_2}}\right] \qquad (5)$$

m=2,4,6,..... The first several of these points are shown in Figure 2. These points are again first-order branch points for the mode pair consisting of a mode and its negative [*Hanson and Yakovlev*, 1998]. The three branch point types, $\omega_m^{(0)}$,$\omega_m^{(1)}$ and $\omega_{m/m+2}^{(2)}$, are depicted in Figure 2. The generalized cutoff frequency loci and the branch points $\omega_m^{(0)}$ and $\omega_{m/m+2}^{(2)}$ in the upper half frequency plane separate the second- and fourth-quadrant modes ($\lambda_m^{(-)}$,$-\lambda_m^{(-)}$) in Figure 3, whereas those points and loci in the lower half frequency plane separate the first- and third-quadrant modes, ($\overline{\lambda}_m^{(-)}$, $-\overline{\lambda}_m^{(-)}$) from Figure 3 (which are analytically continued as the modes ($\lambda_m^{(-)}$,$-\lambda_m^{(-)}$)). Note that the complex-frequency-plane is infinitely sheeted, with branch points generally connecting only certain sheets.

It can be seen that complex-frequency-plane analysis for the TM^z-even modes is very complicated. All modes are analytically connected to one another such that any mode can be smoothly changed into any other mode by the appropriate frequency path, motivating the notation $\lambda_{m(\Omega)}(\Omega)$, where $m(\Omega)$must imply dependence of the mode number not only on the point in parameter space, but also on the particular path taken from $0 \in \mathbb{C}^4$ to $\Omega \in \mathbb{C}^4$. It is important to note that the observed behavior is believed typical for TM^z-even modes but is based on numerical solutions for the specific geometry described in the caption of Figure 2. Numerical values for the first several branch points $\omega_m^{(0)}$,$\omega_m^{(1)}$,$\omega_{m/m+2}^{(2)}$ and the points ω_m^c are listed in Table 1.

It seems that the complicated modal behavior concerning $\omega_{m/m+2}^{(2)}$ and the generalized cutoff loci, described above for lossless media, has not been described in detail previously (the points $\omega_m^{(0)}$,$\omega_m^{(1)}$ were also discussed by *Hanson and Yakovlev*, [1998]). The reason is probably that generally one is concerned with time-harmonic phenomena, wherein frequency is varied along the real axis. Under this restriction the branch points $\omega_m^{(0)}$ and $\omega_{m/m+2}^{(2)}$ are never encountered. When material loss or gain is introduced, all branch points migrate in the complex-frequency-plane as depicted in Figure 6 for the fourth-quadrant points $\omega_m^{(0)}$ and $\omega_{m/m+2}^{(2)}$ and the points $\omega_m^{(1)}$. In Figure 6 it can be seen that all of the branch points move from their initial positions into the first quadrant as loss is increased. The effect of the migration of the branch points $\omega_m^{(1)}$ with loss was described by *Hanson and Yakovlev* [1998]. This observation explains the characteristics of the "spectral gap" in the lossy media case [*Shigesawa* et al., 1993]. The migration of the branch points $\omega_{m/m+2}^{(2)}$, particularly for loss values which cause the branch points to cross the real-frequency axis,

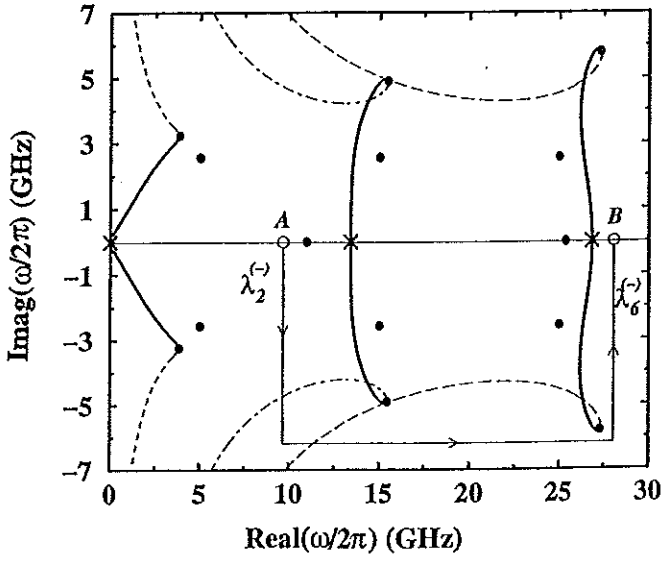

Figure 5b. Example of a complex-frequency-plane path which results in the transformation of the $\lambda_2^{(-)}$ mode into the $\lambda_6^{(-)}$ mode.

Table 1. Complex-Frequency-Plane Branch Points $\omega_m^{(0)}, \omega_m^{(1)}, \omega_{m/m+2}^{(2)}$ and Cutoff Frequencies ω_m^c for TM-Even Modes of the Symmetric-Slab Waveguide Depicted in Figure 1

m	$\omega_m^{(1)}/2\pi$,	$\omega_{m/m+2}^{(2)}/2\pi$, Ghz	$\omega_m^{(0)}/2\pi$,	$\omega_m^c/2\pi$,
0	...	$\omega_{0/2}^{(2)}/2\pi$=(3.8483, ∓ 3.2403)	...	(0,0)
2	(10.9648,0)	$\omega_{2/4}^{(2)}/2\pi$=(15.4496, ∓ 4.8926)	(5, ± 2.5615)	(13.4164,0)
4	(25.3669,0)	$\omega_{4/6}^{(2)}/2\pi$=(27.3016, ∓ 5.7920)	(15, ± 2.5615)	(26.8328,0)
6	(39.2007,0)	$\omega_{6/8}^{(2)}/2\pi$=(39.2348, ∓ 6.4173)	(25, ± 2.5615)	(40.2492,0)

Here $n_1 = 1, n_2 = 1.5$ and d=2 cm.

results in mode coupling between proper modes. This phenomenon is of primary interest here and is explained in detail below. The migration of the $\omega_m^{(0)}$ points across the real-frequency axis also causes mode coupling, but primarily for improper modes. This is shown in Figure 7, where the modes $\pm\lambda_2$ are shown. The mode trajectory in the propagation-constant plane is shown, parameterized by frequency. With $\epsilon_2 = (\epsilon_2^{/} + j\epsilon_2^{//})\epsilon_0$, dispersion behavior is shown for $\epsilon_2^{//}$= -1.6 (-1.7) such that $\omega_2^{(0)}$ is below (above) the real-frequency axis. Completely different behavior is obtained depending on the loss value. The loss value $\epsilon_2^{//}$=-1.66 places $\omega_2^{(0)}$ on the real-frequency axis and results in the two dispersion curves for $\pm\lambda_2$ becoming degenerate at λ=0.

When gain rather than loss is varied, all three types of branch points migrate in the fourth quadrant as shown, such that the $\omega_m^{(0)}$ and $\omega_{m/m+2}^{(2)}$ points never cross the real-frequency axis and induce coupling. To determine the migration of the first-quadrant points $\omega_m^{(0)}$ and $\omega_{m/m+2}^{(2)}$ under loss or gain variation, recall that the first-quadrant branch points influence the conjugate of the modes which are affected by the fourth-quadrant branch points. Conjugating (1) then shows that the first-quadrant branch points migrate into the fourth quadrant with gain and remain in the first quadrant for loss. Diagrams similar to

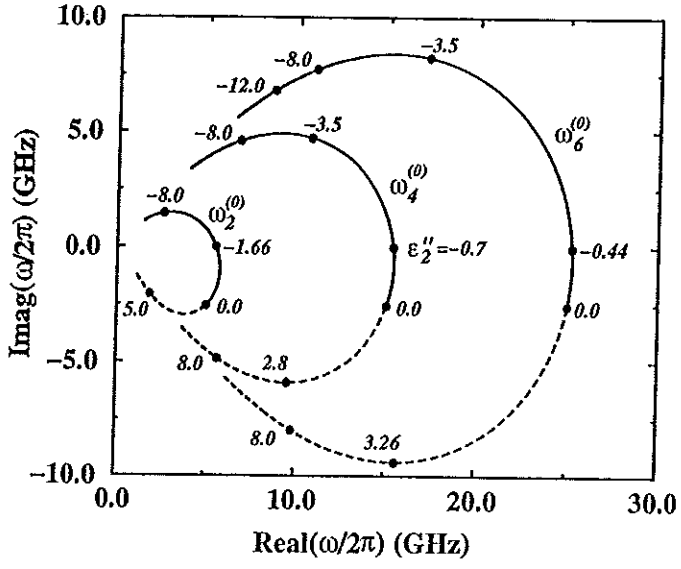

Figure 6a. Migration of the first several fourth-quadrant branch points $\omega_m^{(0)}$ (see Figure 2) in the complex-frequency plane parameterized by $\epsilon_2^{//}$, the imaginary part of the relative permittivity. Migration across the real-frequency axis results in interaction of leaky modes.

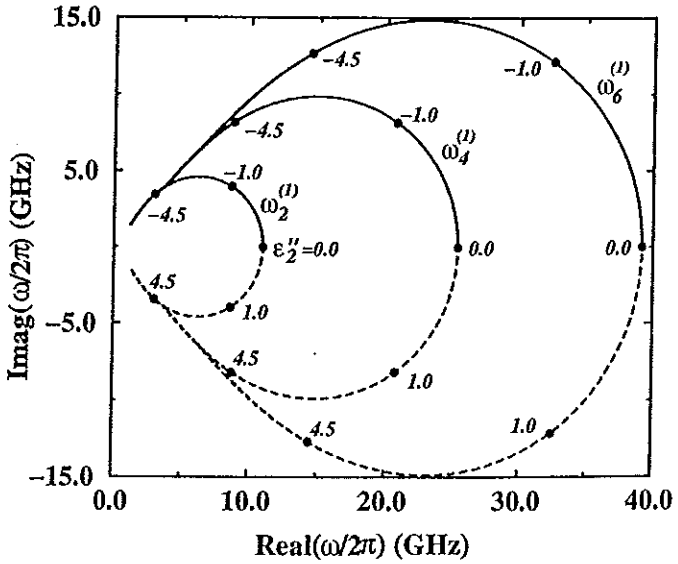

Figure 6b. Migration of the first several branch points $\omega_m^{(1)}$ (see Figure 2) in the complex-frequency-plane parameterized by $\epsilon_2^{//}$.

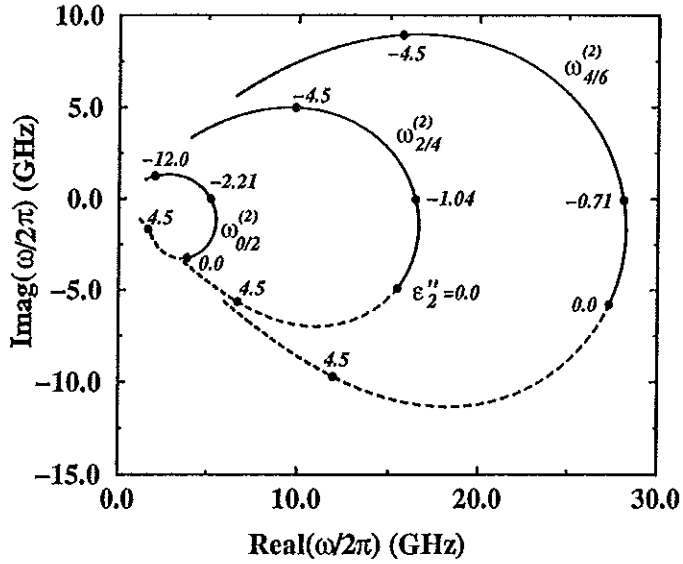

Figure 6c. Migration of the first several fourth-quadrant branch points $\omega^{(2)}_{m/m+2}$ (see Figure 2) in the complex-frequency plane parameterized by ϵ''_2. Migration across the real-frequency axis results in interaction of proper modes.

Figures 6a and 6c for these points can then be formed simply by conjugating the data in Figures 6a and 6c, respectively, and are omitted here.

As an example of coupling induced when the $\omega^{(2)}_{m/m+2}$ branch points migrate across the real-frequency axis, consider the following computational experiment [*Van Stralen et al.*, 1997]. Assume that $\omega, \epsilon_1, \epsilon'_2$ are fixed real numbers with $\epsilon_2=(\epsilon'_2+j\epsilon''_2)\epsilon_0$. Let an initial point in parameter space be given by $\Omega_a=\omega, d_a, \epsilon_1, \epsilon'_2, \epsilon''_{2,a}$, and let $\Omega_b=\omega, d_b, \epsilon_1, \epsilon'_2, \epsilon''_{2,b}$ represent a final point, where $\epsilon''_2<0$ for lossy media, $|\epsilon''_{2,a}|<|\epsilon''_{2,b}|$, and $d_{2,a}<d_{2,b}$. Variation in parameter space $\Omega_a \rightarrow \Omega_b$ can be achieved by first increasing thickness $d_a \rightarrow d_b$ and then increasing loss, $\epsilon''_{2,a} \rightarrow \epsilon''_{2,b}$, method I, or by first increasing loss and then increasing thickness, method II (note that in this example, taken from the optical literature, thickness rather than frequency is varied. Since the eigenvalue transcendental equation (1) can be expressed in terms of normalized wavenumber λ/k_0 and the product $k_0 d$, only the product $k_0 d$ is important, not which parameter (frequency of thickness) is varied.). It can be seen from Figures 8a-8d, that method I leads to the smooth transformation $\lambda_0^{(+)}(\Omega_a) \rightarrow \lambda_0^{(+)}(\Omega_b)$, $\lambda_2^{(+)}(\Omega_a) \rightarrow \lambda_2^{(+)}(\Omega_b)$ while method II leads to a different smooth transformation, $\lambda_0^{(+)}(\Omega_a) \rightarrow \lambda_2^{(+)}(\Omega_b)$, $\lambda_2^{(+)}(\Omega_a) \rightarrow \lambda_0^{(+)}(\Omega_b)$. That is, starting with the lower point d=0.25 cm on the left side of Figure 8a, method I yields the smooth continuation of this mode to reside on the upper curve of Figure 8d. Method II yields the smooth continuation of this same mode to be on the lower curve of Figure 8d. Thus the order in which parameters are varied, in addition to the final value of parameters, determines the mode's wavenumber value. This seemingly nonunique behavior was identified by *Van Stralen et al.* [1997], but its cause was not determined. With the aid of Figures 2 and 6, one can see that this behavior is due to passing over or under the frequency-plane (equivalently, the d-plane) branch points $\omega^{(2)}_{m/m+2}$. If loss is increased first, then frequency or d (method II), the path of parameter variation passes below $\omega^{(2)}_{m/m+2}$, while if frequency or d is increased first, then loss increased (method I), the path passes above $\omega^{(2)}_{m/m+2}$. The difference in passing above or below the branch point is equivalent to encircling the point, resulting in the interchange of modes. Figure 8c depicts the situation when loss attains the critical value which places the branch point $\omega^{(2)}_{0/2}$ on the real d axis, such that when d is increased the modes $\lambda_0^{(+)}$, $\lambda_2^{(+)}$ meet for some value of d. Figure 9 shows similar behavior for the modes $\lambda_2^{(+)}$, $\lambda_4^{(+)}$. Note from Figure 6 that although the media must be considerably lossy for the low-order modes to interact, the higher-order modes tend to begin to interact for

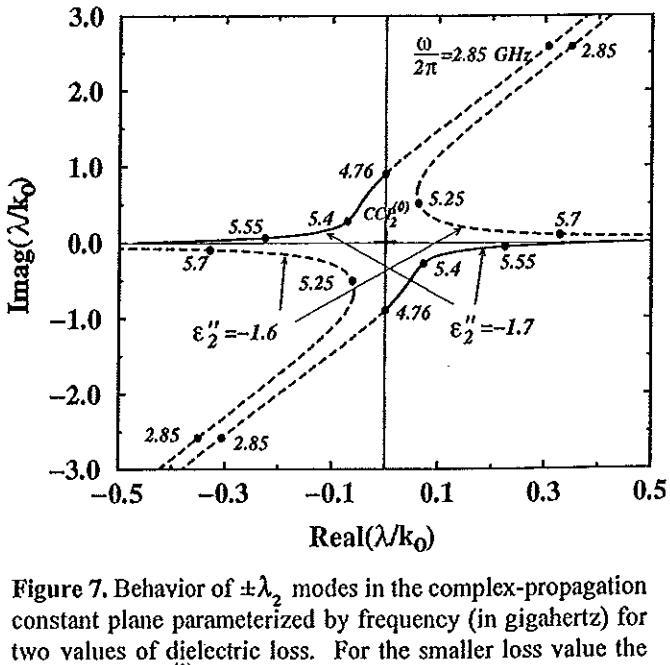

Figure 7. Behavior of $\pm\lambda_2$ modes in the complex-propagation constant plane parameterized by frequency (in gigahertz) for two values of dielectric loss. For the smaller loss value the branch point $\omega_2^{(0)}$ is below the real-frequency axis (see Figure 6a) such that the path of frequency variation along the real axis passes above the branch point. For the larger loss value the frequency path passes below the branch point. The solid (dashed) lines indicate the mode is on the proper (improper) Riemann sheet.

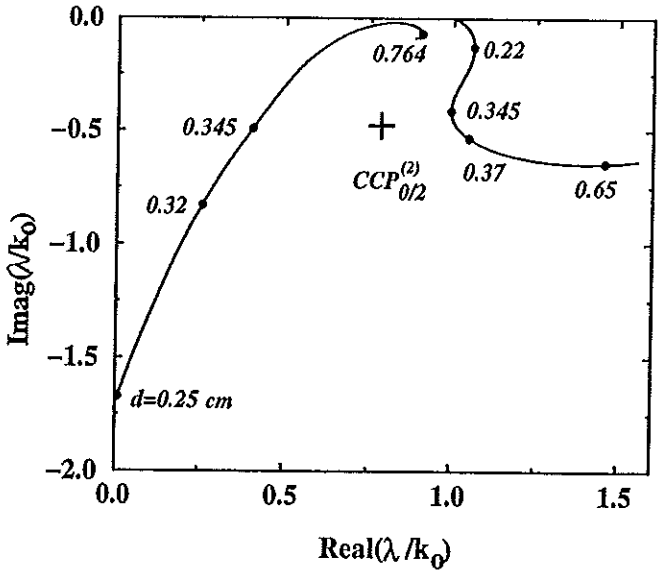

Figure 8a. Propagation constant trajectories for the first two low-order slab modes, parameterized by slab thickness d (centimeters), with frequency held constant at $\omega/2\pi = 30$ GHz and $\epsilon_2'' = -2.0$, such that the fourth-quadrant branch point $\omega_{0/2}^{(2)}$ is below the real d axis.

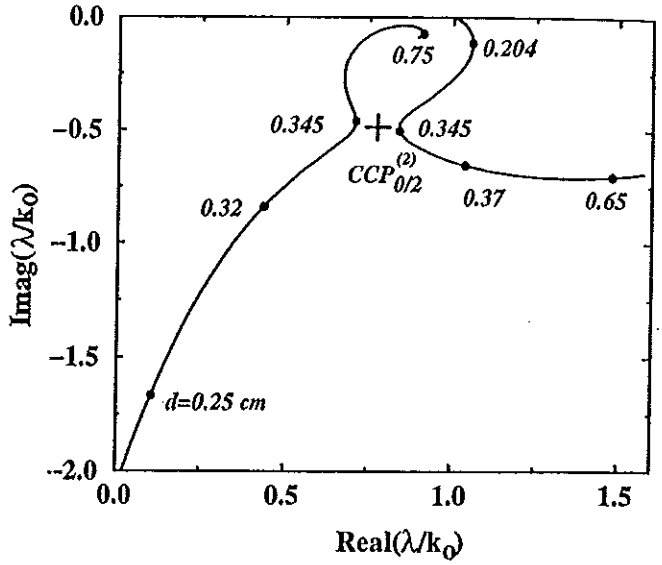

Figure 8b. Similar to Figure 8a, but with $\epsilon_2'' = -2.2$, such that the fourth-quadrant branch point $\omega_{0/2}^{(2)}$ is below, but close to, the real d axis. Modes are beginning to couple together.

smaller values of loss or gain, implying that even in low-loss/low-gain waveguides the higher-order modes couple together.

It can be noted that all branch points discussed here occur when two first-order roots of (1) coalesce to become a second-order root, which indicates that the branch point will satisfy

$$H(\lambda_m, \omega_m^{(i)}) = H_\lambda'(\lambda_m, \omega_m^{(i)}) = 0 \tag{6}$$

$i=0,1,2$. Note that (6) defines a complex pair $(\lambda_m, \omega_m^{(i)})$. The branch points $\omega_m^{(i)}$ are labeled as solid circles in the frequency-plane figures (Figures 2,5,6, and 7). The complex propagation-constant value at the branch point

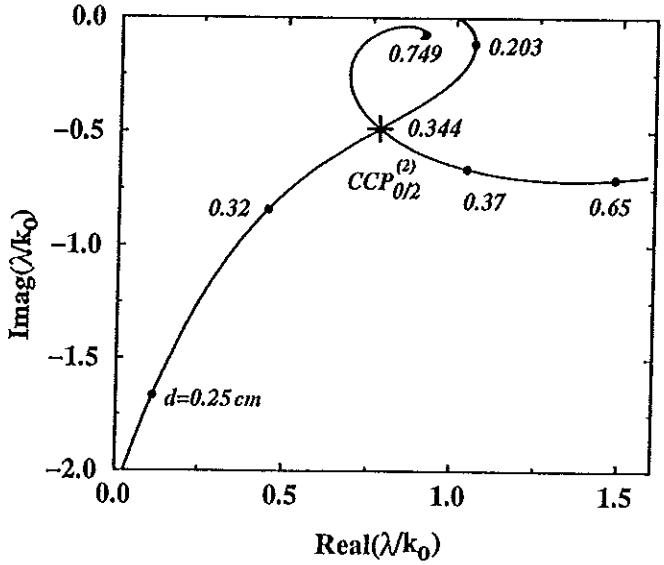

Figure 8c. Propagation constants for critical value of loss $\epsilon_2'' = -2.21286$. The branch point $\omega_{0/2}^{(2)}$ is on the real d axis such that the two modes intersect (become degenerate) at $d=0.344$ cm.

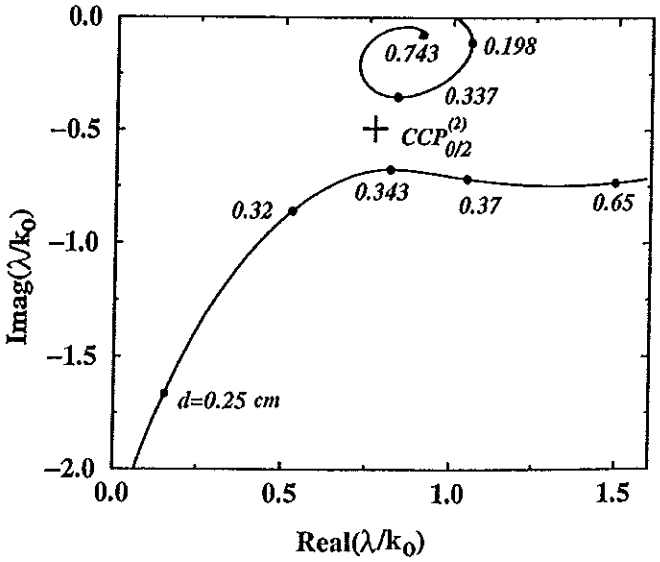

Figure 8d. Propagation constant trajectories for $\epsilon_2'' = -2.3$, such that the branch point $\omega_{0/2}^{(2)}$ is above the real d axis. By considering Figures 8a-8d, one can see that value of propagation constant depends on the order in which the variables (d or ϵ_2'') are varied.

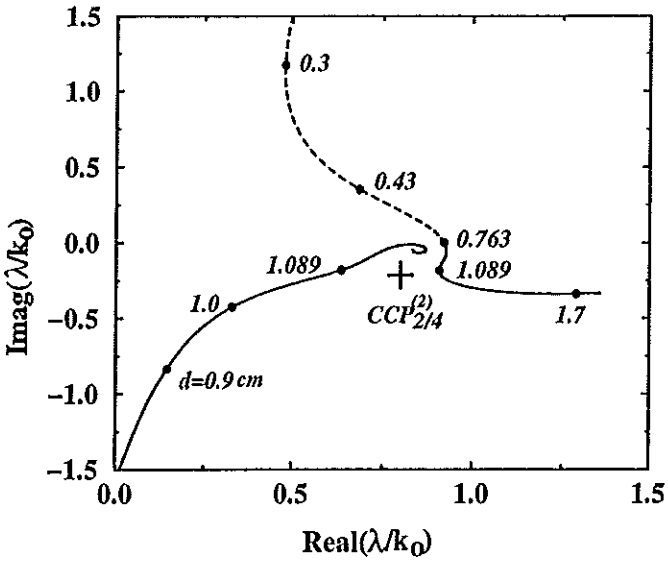

Figure 9a. Propagation constant trajectories for the next higher pair of modes, parameterized by slab thickness d, with frequency held constant at $\omega/2\pi = 30$ GHz and $\epsilon_2'' = -0.95$, such that the fourth-quadrant branch point $\omega_{2/4}^{(2)}$ is below the real d axis. The solid (dashed) lines indicate the mode is on the proper (improper) Riemann sheet.

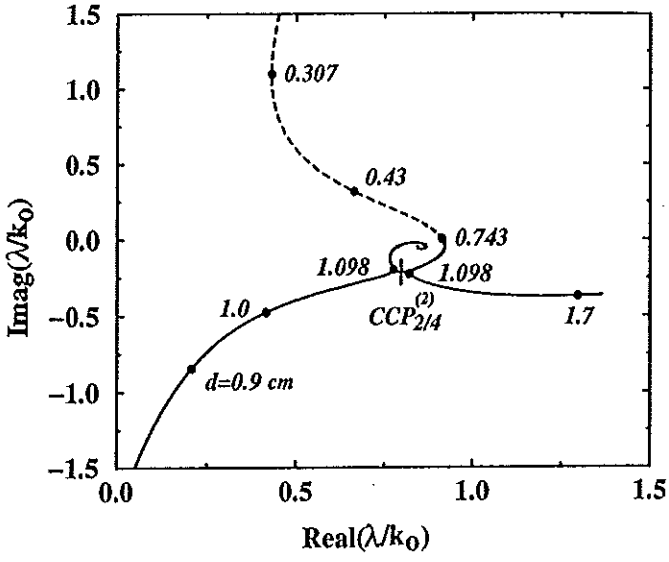

Figure 9b. Similar to Figure 9a, but with $\epsilon_2'' = -1.04$, such that the fourth-quadrant branch point $\omega_{2/4}^{(2)}$ is below, but close to, the real d axis. Modes are beginning to couple together.

frequency is denoted by CCP in Figures 8 and 9, consistent with notation of *Yakovlev and Hanson* [1997]. Although many authors [e.g., *Haddon*, 1986; *Duffy*, 1994; *Ilyinsky* et al., 1993], state that (6) indicates branch point behavior, we point out [*Hanson and Yakovlev*, 1998] that (6) guarantees nothing more than a double root. We have shown that these types of branch points satisfy (6) together with the additional conditions

$$H_{\omega}'(\lambda_m, \omega_m^{(i)}) H_{\lambda\lambda}''(\lambda_m, \omega_m^{(i)}) \neq 0, \tag{7}$$

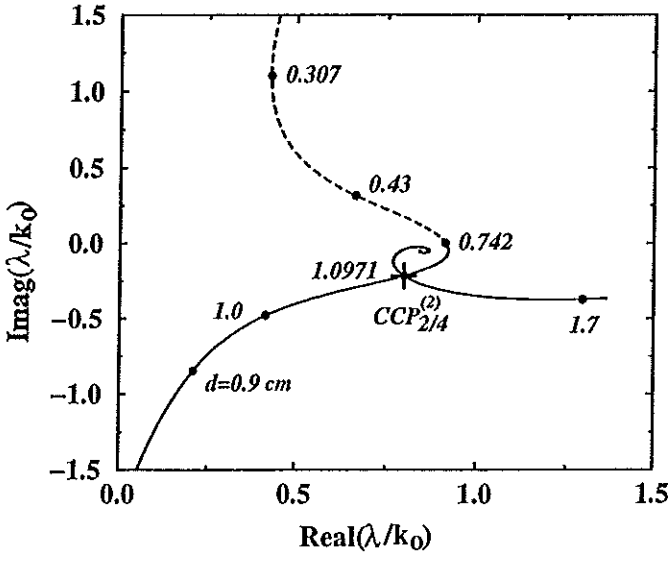

Figure 9c. Propagation constants for critical value of loss $\epsilon_2'' = -1.04308$. The branch point $\omega_{2/4}^{(2)}$ is on the real d axis such that the two modes intersect (become degenerate) at $d = 1.097$ cm.

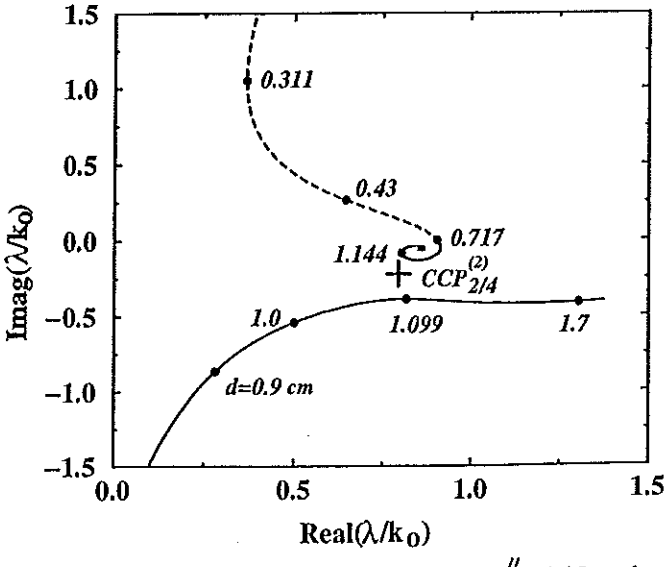

Figure 9d. Propagation constant trajectories for $\epsilon_2'' = -1.15$, such that the branch point $\omega_{2/4}^{(2)}$ is above the real d axis. By considering Figures 9a-9d, one can see that value of propagation constant depends on the order in which the variables (d or ϵ_2'') are varied.

which are sufficient to guarantee that the pair $(\lambda_m, \omega_m^{(i)})$ form a branch point in the ω plane.

A brief comment is in order concerning TE^z-odd modes, which may propagate on the symmetric-slab waveguide and on the grounded dielectric slab. These modes have $\omega_m^{(0)}$ branch points given by (5) (actually, one should count these modes as m=1,3,5,... and replace (m-1) in (5) with m), and cutoff frequencies governed by (4), with m=1,3,5,.... Generalized cutoff loci exist but do not terminate at $\omega_{m/m+2}^{(2)}$ branch points, which do not seem to exist for TE^z-odd modes. Rather, the generalized cutoff loci tend asymptotically toward the imaginary frequency axis.

Note also that the described phenomenon does not occur on simple shielded structures, like the homogeneously filled parallel-plate waveguide of thickness d. In this case, the dispersion function is analytically obtained as $\lambda_m(\omega) = \pm\left[\omega^2\epsilon\mu - (m\pi/2d)^2\right]^{1/2}$, $m = 0, \pm1, \pm2, \ldots$. In the lossless case the only branch points which may occur clearly reside on the real-frequency axis.

3. Conclusion

The cause of TM^z-even mode coupling on planar symmetric-slab waveguides with loss or gain has been investigated by analyzing the migration of complex-frequency-plane branch points of the dispersion function. It was found that several types of frequency-plane branch points occur for the symmetric-slab waveguide and are associated with different wave phenomena. The branch points which cause coupling of the proper modes normally reside in the complex-frequency plane for lossless media, such that they are never encountered in time-harmonic analyses. As loss or gain is introduced, these points may migrate across the real-frequency axis, resulting in mode interaction and exchange. As a result of this branch point migration, the association of a particular mode with a certain branch of the dispersion function depends not only on the value of material loss or gain, but also on the order in which physical parameters of the problem are varied.

References

Collin, R.E., *Field Theory of Guided Waves*, 2nd ed., IEEE Press, Piscataway, N.J., 1991.

Duffy, D.G., Response of a grounded dielectric slab to an impulse line source using leaky modes, *IEEE Trans. Antennas Propag.*, *42*, 340-346, 1994.

Haddon, R.A.W., Exact evaluation of the response of a layered elastic medium to an explosive point source using leaking modes, *Bull. Seismol. Soc. Am.*, *76*, 1755-1775, 1986.

Hanson, G.W., and A.B. Yakovlev, An analysis of leaky-wave dispersion phenomena in the vicinity of cutoff using complex frequency plane singularities, *Radio Sci.*, *33*, 803-819, 1998.

Ilyinsky, A.S., G. Y. Slepyan, and A. Y. Slepyan, *Propagation, Scattering and Dissipation of Electromagnetic Waves*, P. 46, Peter Peregrinus, London, 1993.

Marcuse, D., *Theory of Dielectric Optical Waveguides*, 2nd ed., Academic, San Diego, Calif., 1991.

Niu, F., and L.B. Felsen, Time-domain leaky modes on layered media: Dispersion characteristics and synthesis of pulsed radiation, *IEEE Trans. Antennas Propag.*, *41*, 755-761, June 1993.

Shigesawa, H., M. Tsuji, and A.A. Oliner, The nature of the spectral gap between bound and leaky solutions when dielectric loss is present in printed-circuit lines, *Radio Sci.*, *28*(6), 1235-1243, 1993.

Van Stralen, M.J.N., K.F.I. Haak, and H. Blok, On the classification of discrete modes in lossy planar waveguides: The modal analysis revisited, *Opt. Quantum Electron.*, *29*, 243-262, 1997.

Yakovlev, A.B., and G.W. Hanson, On the nature of critical points in leakage regimes of a conductor-backed coplanar strip line, *IEEE Trans. Microwave Theory Tech.*, *45*, 87-94, Jan. 1997.

Yakovlev, A.B. and G.W. Hanson, Analysis of mode coupling on printed transmission lines using morse critical points, *IEEE Trans. Microwave Theory Tech.*, *46*, 966-974, July 1998.

Yakovlev, A.B. and G.W. Hanson, Mode transformation and mode continuation regimes on waveguiding structures, *IEEE Trans. Microwave Theory Tech.*, in press, 1999.

G. W. Hanson, Department of Electrical Engineering, University of Wisconsin-Milwaukee, 3200 North Cramer Street, Milwaukee, WI 53211. (george@uwm.edu)

A. B. Yakovlev, Department of Electrical and Computer Engineering, North Carolina State University, 1010 Main Campus Drive, 410 EGRC Building, Raleigh, NC 27695. (yakovlev@eos.ncsu.edu)

(Received April 21, 1999; revised August 24, 1999; accepted September 2, 1999.)